Title

Modern brain tumor imaging.

Journal

Brain tumor research and treatment, 3(1)

ISSN

2288-2405

Authors

Mabray, Marc

Barajas, Ramon

Cha, Soonmee

Publication Date

2015-04-01

DOI

10.14791/btrt.2015.3.1.8

Peer reviewed

REVIEW ARTICLE Brain Tumor Res Treat 2015;3(1):8-23 / pISSN 2288-2405 / eISSN 2288-2413
http://dx.doi.org/10.14791/btrt.2015.3.1.8

Modern Brain Tumor Imaging

Marc C. Mabray, Ramon F. Barajas Jr, Soonmee Cha

Department of Radiology and Biomedical Imaging, University of California San Francisco, San Francisco, CA, USA

Received March 16, 2015
Revised March 17, 2015
Accepted March 17, 2015

Correspondence
Marc C. Mabray
Department of Radiology and Biomedical Imaging,
University of California San Francisco,
505 Parnassus Ave, M-391,
San Francisco, CA 94143, USA
Tel: +1-415-502-2866
Fax: +1-415-502-2899
E-mail: marc.mabray@ucsf.edu

The imaging and clinical management of patients with brain tumor continue to evolve over time and now heavily rely on physiologic imaging in addition to high-resolution structural imaging. Imaging remains a powerful noninvasive tool to positively impact the management of patients with brain tumor. This article provides an overview of the current state-of-the art clinical brain tumor imaging. In this review, we discuss general magnetic resonance (MR) imaging methods and their application to the diagnosis of, treatment planning and navigation, and disease monitoring in patients with brain tumor. We review the strengths, limitations, and pitfalls of structural imaging, diffusion-weighted imaging techniques, MR spectroscopy, perfusion imaging, positron emission tomography/MR, and functional imaging. Overall this review provides a basis for understudying the role of modern imaging in the care of brain tumor patients.

Key Words Magnetic resonance imaging; Brain neoplasms; Glioma; Glioblastoma; Neuroimaging.

INTRODUCTION

Modern neuroimaging is critical to the clinical management of patients with brain tumor. Noninvasive neuroimaging techniques now offer the opportunity to incorporate functional, hemodynamic, metabolic, cellular, microstructural, and genetic information into the assessment of brain tumor patients [1-3]. These imaging tools are being applied to diagnose and grade brain tumors preoperatively, to plan and navigate surgery intra-operatively, to monitor and assess treatment response and patient prognosis, and to understand the effects of treatment on the patients brain. Ongoing research in brain tumor imaging attempts to develop, validate, and clinically implement advanced neuroimaging techniques that can aid in the diagnosis and identification of any disease factors or clinically relevant risk factors specific to each patient, the selection and implementation of the appropriate treatment targeting the unique biology of the individual tumor, and the detection of early treatment failure and any early or late onset therapy related complications.

This article provides an overview of the current state-of-the art clinical brain tumor imaging in 2015. We will discuss general magnetic resonance (MR) imaging methods and their application to the diagnosis of, treatment planning and navigation, and disease monitoring in patients with brain tumor. We will review the strengths, limitations, and pitfalls of diffusion-weighted imaging (DWI) techniques, MR spectroscopy (MRS), perfusion imaging, positron emission tomography (PET)/MR, and functional imaging. A detailed discussion of the underlying MR physics is beyond the scope of this clinical review and will only be mentioned briefly when relevant. We intend to discuss the modern clinical application of these methods in the daily evaluation and treatment of patients with brain tumor.

BRAIN TUMOR BIOLOGY AND GENETICS

The World Health Organization (WHO) defines four grades of brain tumors based primarily upon tumor aggressiveness with grade I tumors being relatively non-aggressive and grade IV tumors being very aggressive [4]. Traditionally with the first edition in 1979, WHO grades were assigned on the basis of histologic features such as mitotic activity, necrosis, and infiltration [5]. The second edition, in 1993, incorporated immunohistochemistry, and the third edition in 2000 incorporated genetic profiles into the definitions of brain tumors [6,7]. The most recent WHO central nervous system (CNS) tumor classification system was published in 2007 and continues to inte-

grate genetic profiles into tumor definitions and histological variants [4]. Genetics and molecular profiles of brain tumors continue to be an active area of research with diagnostic, prognostic, therapeutic, and imaging implications [2,8,9]. Here we review the main relevant molecular and genetic aberrations in brain tumors that are relevant to understanding individual variations in tumor biology, response to therapy, and prognosis. An overview is provided in Table 1.

TP53

The p53 tumor suppression pathway is commonly abnormal in high-grade gliomas. The p53 gene (*TP53*) has been reported to be mutated in approximately 30−40% and the overall pathway has been reported to be disrupted in more than 80% of tumors [2,9-11]. The p53 protein is involved in DNA repair, arresting the cell cycle for DNA repair when there is DNA damage, and in initiating apoptosis. Abnormalities in the p53 tumor suppression pathway can lead to genetic instability, reduced apoptosis, and angiogenesis. The p53 tumor suppression pathway may be disrupted by mutation or deletion of the *TP53* gene or by overexpression of inhibitors of p53 including murine double minute 2 which may result by direct mutation or by mutation of cyclin-dependent kinase inhibitor 2A (*CDKN2A*) [2,9,11].

RB1

The retinoblastoma 1 (*RB1*) tumor suppression pathway is commonly abnormal in glioblastoma, and is disrupted in more than 75% of tumors [2,9]. Rb1 is a protein that blocks cell cycle progression and if the pathway is abnormal there may be unchecked cell cycle progression [2]. The Rb1 tumor suppression pathway may be disrupted by a direct mutation of the *RB1* gene or by overexpression of cyclin-dependent kinase 4 (*CDK4*). Overexpression of *CDK4* may result from amplification or more commonly through deletion of an inhibitor of *CDK4*, *CDKN2A* [2,9,11].

EGFR and *PTEN*

The epidermal growth factor receptor (EGFR) is a trans-membrane receptor in the receptor tyrosine kinase (RTK), phosphatase and tensin homolog (PTEN), phosphatidylinositol 3-kinase (PI3K) cell proliferation pathway [2]. *EGFRvIII*, a mutated form of *EGFR*, plays a prominent role in tumorigenesis of glioblastoma, but the underlying mechanisms have remained elusive. *EGFRvIII* amplification can lead to increased downstream activity resulting in proangiogenic signaling, increased proliferation, increased tumor cell survival, and migration [2]. *EGFRvIII* amplifications have been reported in approximately 40% of primary glioblastomas [4,8,12]. *EGFRvIII* amplification has been reported to be a predictor of poor survival, however, other studies have failed to show this effect [4,8,13,14]. Studies have reported that *EGFRvIII* amplification can predict response to tyrosine kinase inhibitors, especially when *PTEN* expression is preserved [15].

PTEN is a tumor suppressor gene expressing a protein involved in the same RTK/PTEN/PI3K cell proliferation pathway as *EGFR* [2]. *PTEN* mutations are estimated to occur in 15−40% of primary glioblastomas but up to 80% of glioblas-

Table 1. Genetic mutations in brain tumors with current clinical and imaging implications

Genetic mutations and clinical imaging implications/associations		
	Current implications/associations	Imaging associations
IDH1/2 mutations	Oligodendroglial tumors Positive prognostic factor	Minimal or no contrast enhancement Reported detection of 2-HG by MRS Research into hyperpolarized C13 detection in animal models
1p19q deletion	Oligodendroglial tumors	Reported more heterogeneous signal characteristics Reported elevated perfusion
MGMT promoter methylation	Pseudo-progression more common Alkylating agents	Pseudo-progression more common
ATRX deletion	Astrocytic tumors Not seen with 1p19q deletion	
PTEN deletion	Small cell phenotype of glioblastoma with *EGFR* amplification and 10q loss	Reported increased perfusion in tumors with *PTEN* mutation, *EGFR* amplification, unmethylated *MGMT* promoter
EGFR amplification	Reported in approximately 40% of glioblastomas	Reported increased perfusion Reported lower ADC values, higher enhancing/necrotic volume

ADC, apparent diffusion coefficient; *ATRX*, alpha thalassemia-mental retardation syndrome X-linked; C-13, carbon 13; *EGFR*, epidermal growth factor receptor; *IDH*, isocitrate dehydrogenase; *MGMT*, O^6-methylguanine-DNA methyl-transferase; MRS, magnetic resonance spectroscopy; *PTEN*, phosphatase and tensin homolog; 2-HG, 2-hydroxyglutarate

tomas have loss of chromosome 10q in the region where *PTEN* is located (10q23) [8,16]. Chromosome 10q loss, *PTEN* mutations, and *EGFR* amplification are frequently seen together in the small cell phenotype of glioblastoma [4,8]. *PTEN* deletions have been reported to be a poor prognostic factor for pediatric glioblastomas, however, this has not been found true in adult patients [8,17].

Several magnetic resonance imaging (MRI) parameters have been reported as predictive of *EGFR* amplification. A high ratio of contrast enhancing tissue to necrotic tissue (≥1), lower apparent diffusion coefficient (ADC) values, increased T2 to contrast enhancing volume, and deceased T2 border sharpness have all been described with *EGFR* amplification [2,18-20]. In addition, increased normalized tumor blood volume has been reported in tumors with *EGFR* amplification, *PTEN* deletion, and normal unmethylated O^6-methylguanine-DNA methyltransferase (*MGMT*) [21].

IDH1/*IDH2*

Isocitrate dehydrogenase 1 and 2 (IDH1 and IDH2) are enzymes involved in the citric acid cycle. *IDH1* gene mutations are seen in about 5% of patients with primary glioblastoma but are seen in 70−80% of grade II−III gliomas and secondary glioblastomas (glioblastomas arising from low grade gliomas) [2,8,22-24]. IDH2 mutations are mostly seen in oligodendroglial tumors [8,24]. Patients with *IDH1/2* mutations have been reported to have better survival independent of therapy [23-26]. On imaging *IDH1* mutated tumors are reported to be more likely to be multi-focal, invasive, and have minimal or no contrast enhancement [2,27,28]. The mutant IDH1 and 2 enzymes have shown neomorphic enzymatic capacity to covert alpha-ketoglutarate into 2-hydroxy-glutarate (2-HG), a small oncometabolite. Detection and semi-quantitation of 2-HG by proton MRS has been reported and this noninvasive detection of 2-HG oncometabolite may prove to be a valuable diagnostic and prognostic biomarker [29].

1p/19q

Co-deletion of chromosomes 1p and 19q results from an unbalanced centromeric translocation and is considered indicative of oligodendroglial lineage [8]. 1p/19q co-deletion is seen in approximately 80% of oligodendrogliomas, 60% of anaplastic oligodendrogliomas, 30−50% of oligoastrocytomas, and 20−30% of anaplastic oligoastrocytomas and is frequently seen with *IDH1/2* mutations [8,30,31]. 1p/19q co-deletion has been reported as a favorable prognostic factor and to indicate patients who would benefit from chemoradiation although this significance may be complicated by the frequency of favorable *IDH1/2* mutations and unfavorable additional chromosomal mutations [26,32-36]. This prognostic significance likely depends on the type of 1p loss, with partial 1p losses being associated with poorer survival than complete 1p losses [37]. 1p/19q co-deleted tumors have been reported to be more likely to have indistinct/irregular margins and more heterogeneous T1 and T2 signal characteristics than tumors of the same histology but with 1p/19q intact although the differences were modest and subjective [38]. Elevated perfusion has also been suggested in low-grade oligodendrogliomas with 1p/19q loss although in small studies [39,40].

MGMT

MGMT is a DNA repair protein involved in repairing damage induced by alkylating agents [8,36]. Methylation of the *MGMT* gene promoter reduces binding of transcription factors and decreases gene expression [41]. Methylation thus theoretically increases sensitivity to alkylating chemotherapeutics [42]. *MGMT* promoter methylation is reported to be present in 35−75% of glioblastomas [8,42]. Multiple studies have shown a better prognosis and response for glioblastoma patients with *MGMT* promoter methylation receiving temozolamide [42-45]. Pseudo-progression after radiation and chemotherapy is more common in tumors with *MGMT* promoter methylation and *MGMT* promoter methylation should be this taken into account when interpreting follow-up MRIs [46,47].

BRAF

BRAF is a proto-oncogene that encodes the protein B-Raf, which is involved in the mitogen-activated protein kinase pathway [8,48]. This pathway is involved in cell proliferation, differentiation, survival, and apoptosis. Activating *BRAF* mutations are seen in numerous malignancies, most frequently however in melanoma [49]. Pilocytic astrocytomas have been shown to have *BRAF* mutations with a specific duplication/fusion mutation occurring in 65−80% of pilocytic astrocytomas [50,51]. A separate specific point mutation (V600E) is seen in up to 80% of pleomorphic xanthoastrocytomas and 25% of gangliogliomas [8,52].

ATRX

The alpha thalassemia-mental retardation syndrome X-linked (*ATRX*) gene encodes a protein that is involved in telomere maintenance in a mechanism that does not involve telomerases known as alternative lengthening of telomeres [36,53,54]. *ATRX* mutations have been reported in tumors of astrocytic lineage [55,56]. *ATRX* mutations are associated with *TP53* and *IDH1* mutations and are generally not seen with 1p/19q co-deletions and are thus useful in distinguishing from tumors of oligodendroglial origin [55-58]. *ATRX* loss has been reported as a favorable prognostic indicator in patients whose tumors also had *IDH1* mutations [59].

Histone H3

Histones are proteins involved in the packaging of DNA. Recently, mutations have been identified in the gene encoding histone 3 (*H3F3A*) in pediatric patients with glioblastomas and pontine gliomas [36,58,60]. These mutations have been reported at distinct locations in the histone variants H3.1 and H3.3, one involving a Lysine (Lys27) in H3.1 and H3.3 and one involving a glycine in H3.3 (Gly34) [58,60,61]. The *H3F3A* Lys27 mutation is reported to have a particularly poor prognosis [57]. These mutations are generally not seen together with *IDH1* mutations and thus represent an alternative group of tumors with distinct molecular aberrations [61].

STRUCTURAL AND HIGH RESOLUTION IMAGING

Computed tomography (CT) may be the first modality employed in a patient presenting with a brain tumor but for the most part MRI is the primary imaging modality in brain tumor patients. The role of CT is largely relegated to emergent imaging in the detection of hemorrhage, herniation, and hydrocephalus but mass effect from brain tumors and calcification within brain tumors such as oligodendrogliomas or menigiomas can potentially be detected (Fig. 1) [62,63].

Structural MRI sequences play a major role in the evaluation of and treatment planning of brain tumors. Standard sequences performed utilizing spin-echo techniques include T2 fluid-attenuated inversion recovery (FLAIR), pre-gadolinium T1, and post-gadolinium T1. These sequences are preferably performed in at least 2-orthogonal planes or obtained with a 3-dimensional (3D) sequence that is reformatted into orthogonal planes (i.e., 3D-T2 FLAIR). High-resolution iso-volumetric sequences such as high-resolution 3D T2 sequences and post-gadolinium T1 spoiled gradient recalled acquisition (SPGR) or similar sequences are generally performed preoperatively with fiducials in place for use with intraoperative navigational software [64,65]. Similarly, post-gadolinium T1 SPGR sequences are performed with a stereotactic head frame in place prior to stereotactic radiosurgery [66,67]. High-resolution 3D T2* gradient echo sequences such as susceptibility weighted imaging (SWI) are also routinely performed. These susceptibility sensitive sequences are very sensitive to blood products and calcification and may be helpful to depict post-radiotherapy microhemorrhages [68-70].

The primary roles of structural MRI in initial brain tumor evaluation includes determining the location of the lesion (i.e., intra-axial vs. extra-axial), establishing the specific location within the brain for treatment/biopsy planning, evaluating mass

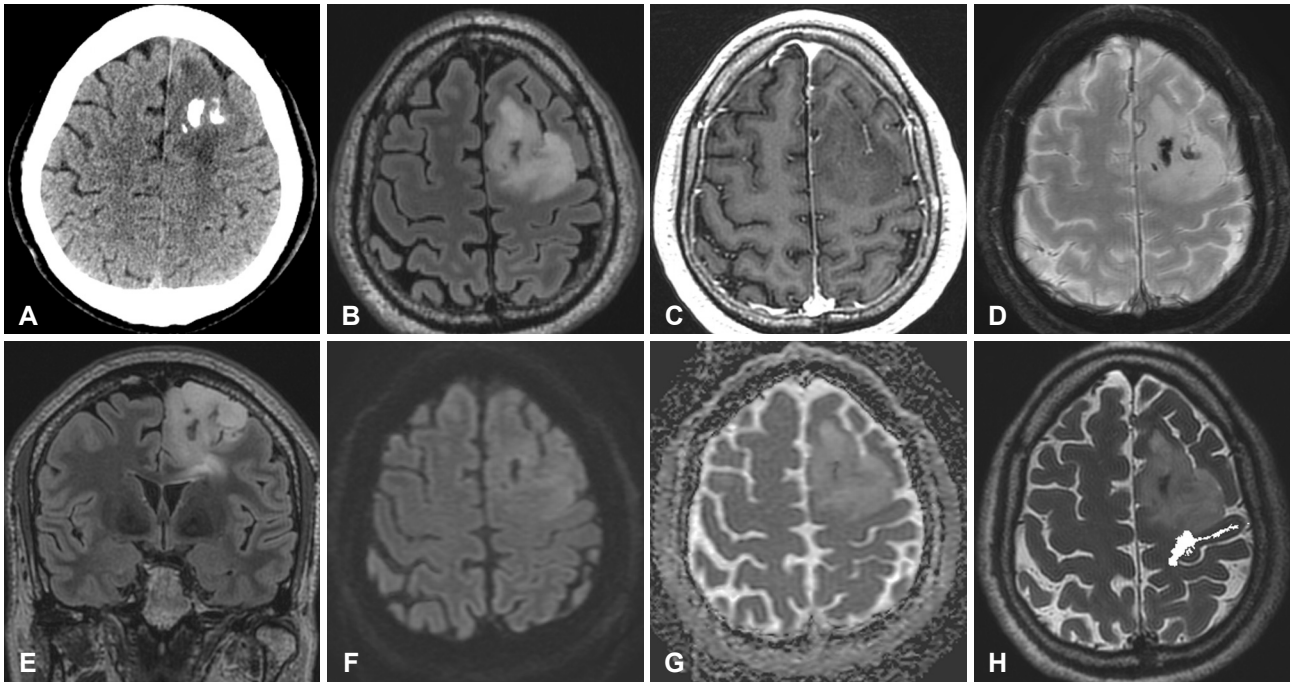

Fig. 1. 57-year-old male patient who presented with loss of consciousness and seizure and who initially had a non-contrast CT (A) performed that demonstrated a partially calcified mass in the left frontal lobe. Preoperative MR images include axial T2 FLAIR (B), axial T1 post-contrast (C), axial SWI (D), coronal T2 FLAIR (E), axial DWI (F), axial ADC map (G), and DTI tractography of the left corticospinal tract superimposed on axial T2 (H). This T2/FLAIR hyperintense (B, E, and H), non-enhancing mass (C), with internal calcifications visible on CT (A) and as susceptibility on SWI (D) was a grade II oligoastrocytoma (*TP53* mutation negative, *IDH1* mutation positive, 1p19q co-deletion positive). A gross total resection was performed and the patient remains alive. ADC, apparent diffusion coefficient; CT, computed tomography; DTI, diffusion-tensor imaging; DWI, diffusion weighted imaging; FLAIR, fluid attenuated inversion recovery; MR, magnetic resonance; SWI, susceptibility weighted imaging.

effect on the brain, ventricular system, and vasculature, and along with physiologic MRI sequences suggesting a possible diagnosis. Extra-axial tumors such as meningiomas, schwannomas, and skull base tumors can generally but not always be differentiated from intra-axial tumors. The differential diagnosis for intra-axial tumors depends on patient age and the presence of another primary malignancy [71,72].

Making a diagnosis of a specific tumor type can be challenging but often the correct diagnosis can be suggested in a short list of likely possibilities. Contrast-enhancement signifies local breakdown of the blood brain barrier and is a key feature seen in many brain tumors and other mass lesions (Fig. 2-6). Within gliomas, contrast enhancement is generally considered to be associated with high-grade tumor (Fig. 2, 3) although certain low-grade gliomas such as pilocytic astrocytomas in children generally enhance and certain high-grade gliomas may not enhance [73-77]. Peri-tumoral edema is generally T2/FLAIR hyperintense signal abnormality surrounding the main mass lesion (Fig. 2-4). This may in some instances such as with metastasis (Fig. 4) represent predominately vasogenic edema surrounding the lesion, however with gliomas the peri-tumoral edema generally also represents infiltrative edema with tumor cells infiltrating into the regions of non-enhancing T2/FLAIR signal abnormality [1,78-81]. The number of lesions is an important factor to consider as a large number of lesions may signify certain pathologies such as metastases; however, metastasis can be solitary, as can tumor mimics such as demyelinating lesions or cerebral abscesses [82-87]. Other potentially distinguishing features to note include a cyst and mural nodule morphology (seen with the lower grade tumors hemangioblastoma, pilocytic astrocytoma, ganglioglioma, and pleomorphic xanthoastrocytoma), calcification (Fig. 1) (generally seen with oligodendrogliomas), and necrosis and hemorrhage (generally seen in higher grade gliomas and hemorrhage also in certain metastases) [62,88-90].

Many of the same features are important in the ongoing evaluation of patients with known brain tumors. Per the updated Response Assesment in Neuro-Oncology working group a complete response to therapy for high-grade gliomas is defined as complete resolution of contrast enhancing disease with stable or decreased T2/FLAIR signal abnormality while not on corticosteroids; a partial response is defined as no new lesions, a ≥50% reduction in contrast enhancing disease, and stable or decreased T2/FLAIR abnormality while on stable or decreased dose of corticosteroids; stable disease is defined as no new lesions, <50% decrease but <25% increase in contrast enhancing disease, and stable or decreased T2/FLAIR abnormality while on stable or decreased dose of corticosteroids; and progressive disease is defined as any new lesion, a ≥25% increase in contrast enhancing disease, or increased T2/FLAIR abnormality [91]. These assessment criteria provide a framework for evaluation but do not account for some of the subtleties and nu-

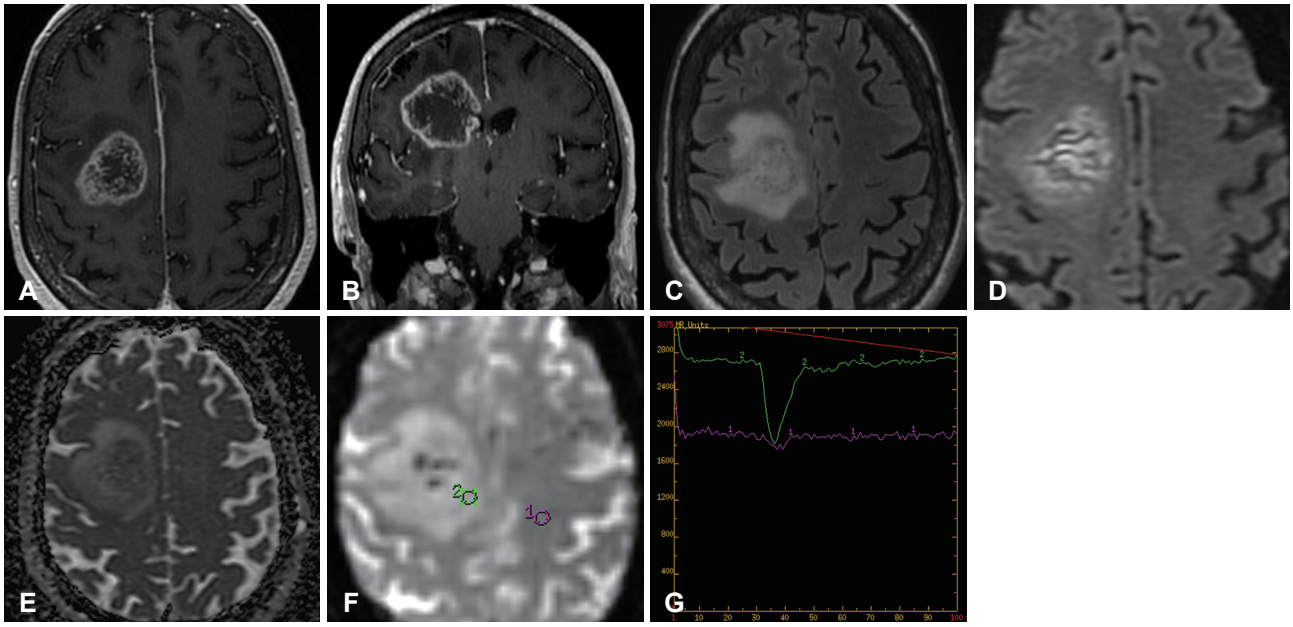

Fig. 2. 78-year-old female patient with a glioblastoma who presented with gait instability, dizziness, and dysarthria for 6–8 weeks. Preoperative MR images include axial T1 post-contrast (A), coronal T1 post-contrast (B), axial T2 FLAIR (C), axial DWI (D), axial ADC map (E), axial DSC perfusion (F), and corresponding perfusion curve (G). Post-contrast T1 images (A and B) demonstrate irregular rim enhancement and central necrosis of this tumor centered in the right frontal lobe. Surrounding the enhancing component is T2 FLAIR hyperintensity (C) which is likely infiltrative cellular edema. The lesion demonstrates restricted diffusion with low ADC values (D and E) and increased relative cerebral blood volume compared to the contralateral side (F and G) with return to baseline of the perfusion curve consistent with a primary glial tumor. ADC, apparent diffusion coefficient; DSC, dynamic susceptibility contrast-enhanced; DWI, diffusion weighted imaging; FLAIR, fluid attenuated inversion recovery; MRI, magnetic resonance image.

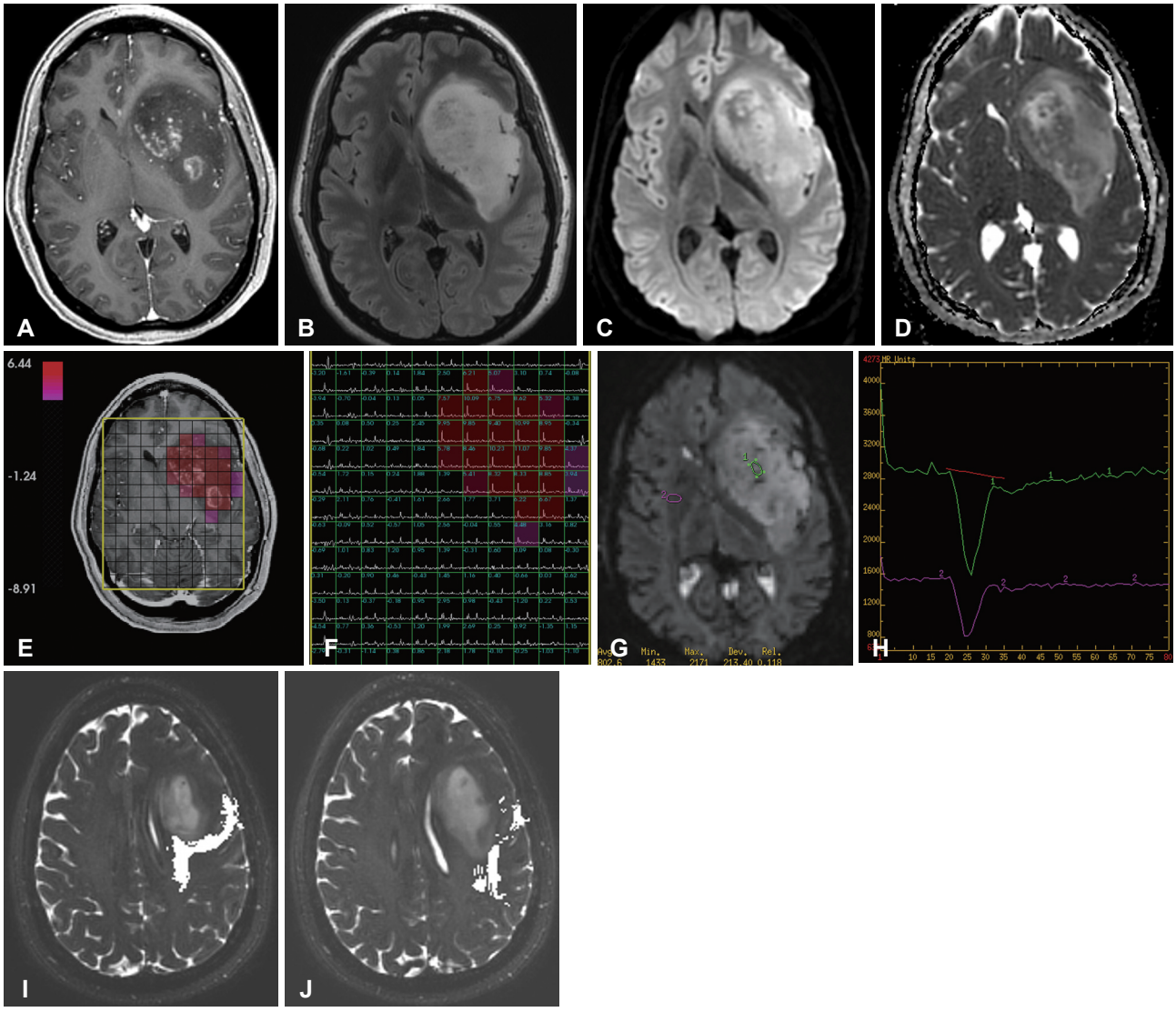

Fig. 3. 33-year-old female patient with a left insular glioblastoma (19q deletion, 1p intact, *IDH1* mutation, *PTEN* and *EGFR* mutation negative) who presented with syncope and seizure. Preoperative MR images include axial T1 post-contrast (A), axial T2 FLAIR (B), axial DWI (C), axial ADC map (D), spectroscopy with choline to NAA ratio overlay on axial T1 post-contrast (E), corresponding spectroscopy and choline to NAA ratios (F), axial DSC perfusion (G), corresponding perfusion curve (H), and DTI tractography of the left corticospinal tract (I) and left arcuate fasciculus (J) superimposed on axial T2. Post-contrast T1 image (A) demonstrate irregular patchy partial enhancement within the tumor. T2 FLAIR (B) shows the extent of non-enhancing T2 FLAIR hyperintense tumor. The lesion demonstrates areas of restricted diffusion with low ADC values (C and D) and increased relative cerebral blood volume compared to the contralateral side (G and H) with return to baseline of the perfusion curve consistent with a primary glial tumor. Spectroscopy (E and F) demonstrates elevated choline relative to NAA, consistent with a glioma. ADC, apparent diffusion coefficient; DSC, dynamic susceptibility contrast-enhanced; DTI, diffusion tensor imaging; DWI, diffusion weighted imaging; *EGFR*, epidermal growth factor receptor; FLAIR, fluid attenuated inversion recovery; *IDH*, isocitrate dehydrogenase; MRI, magnetic resonance image; NAA, N-acetylaspartate; *PTEN*, phosphatase and tensin homolog.

ances of evaluation of the post-treatment brain. A pseudo-response may be seen with a marked decrease in contrast enhancement following treatment with bevacizumab, an antiangiogenic agent uside in recurrent glioblastoma [91-94]. On the other hand, pseudo-progression may be seen as an increase in the contrast enhancing tumor and T2/FLAIR signal abnormality. Pseudo-progression is often associated with radiotherapy and temozolamide where it is seen in around 20% of patients (approximately 1/2 of the patients who initially "progress" on imaging) and may be seen more frequently in tumors with *MGMT* promoter methylation [46,47,91,95,96]. Follow-up studies and physiologic MRI sequences may be useful in the evaluation of pseudo-response and pseudo-progression. T2* based susceptibility sequences such as SWI may show small micro-hemorrhages develop over time in patients who have received radiation therapy [70,97,98]. These small micro-hemorrhages likely indicate delayed toxicity of radiation on the microvasculature of the brain. An overview of imaging techniques

and general major utility is presented in Table 2.

DIFFUSION-WEIGHTED IMAGING

DWI offers insight into the diffusion of water molecules in tissues and can be used to calculate the ADC. DWI is a routine sequence that has become indispensable in the evaluation of stroke but also offers value in the evaluation of brain tumors. ADC values derived from DWI have been shown to be decreas-ed in highly cellular tumors such as CNS lymphoma, medulloblastoma, and high-grade glioma and to be deceased in highly viscous materials such as that within cerebral abscesses [84-87,99-102].

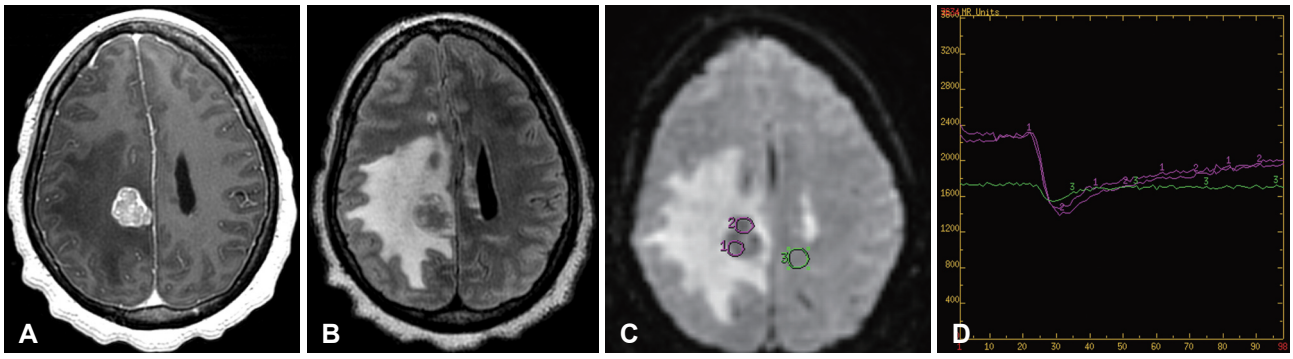

Fig. 4. 49-year-old female patient with two months of headaches and falls and a remote history of right lung lobectomy for reported benign tumor with MR imaging demonstrating a solitary mass in the right cingulate gyrus which upon resection was metastatic adenocarcinoma (ultimately metastatic non-small cell lung cancer). Preoperative MR images include axial T1 post-contrast (A), axial T2 FLAIR (B), axial DSC perfusion (C), and corresponding perfusion curve (D). Post-contrast T1 image (A) demonstrates the solitary enhancing mass. T2 FLAIR (B) shows the large amount of peri-tumoral vasogenic edema. DSC perfusion (C and D) shows elevated cerebral blood volume relative to the contralateral side without return of the curve to baseline, suggesting a solitary metastasis as opposed to a glioma. DSC, dynamic susceptibility contrast-enhanced; FLAIR, fluid attenuated inversion recovery; MRI, magnetic resonance image.

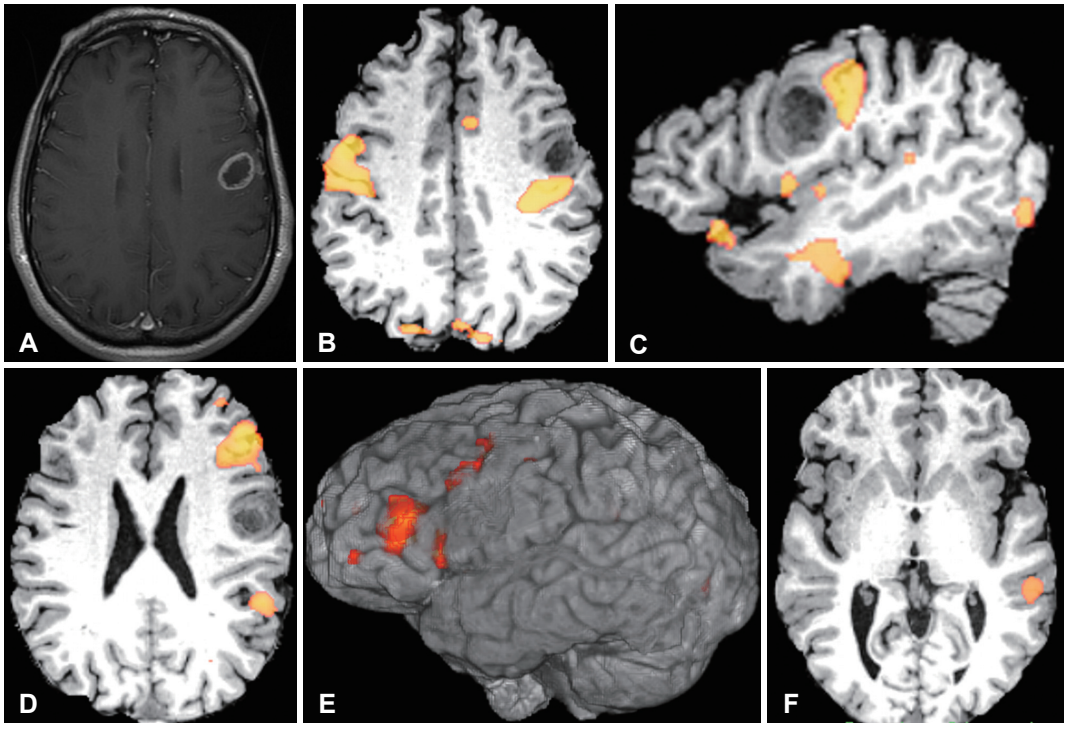

Fig. 5. 64-year-old male patient who presented with expressive aphasia and dysarthria and ultimately was diagnosed with glioblastoma (*IDH1* non-mutated, *PTEN* deleted, *EGFR* amplification negative) and underwent a subtotal resection. Preoperative MR images include axial T1 post-contrast (A) demonstrating a peripherally enhancing mass, and task based BOLD-fMRI functional maps superimposed on anatomic images (B-F) (courtesy of Pratik Mukherjee, MD, PhD). A tongue movement paradigm (B and C) demonstrated bilateral supra-sylvian peri-rolandic activation, which on the left abuts the posterior aspect of the tumor anteriorly as demonstrated on axial (B) and sagittal (C) images. A covert visual verb generation paradigm localized expressive language function to the left (D and E), which was anterior to the tumor but approached the anterior inferior aspect of the tumor (not pictured). A passive listening paradigm localized receptive language function to the left (F), separate from the tumor. *EGFR*, epidermal growth factor receptor; fMRI, functional magnetic resonance image; *IDH*, isocitrate dehydrogenase; MRI, magnetic resonance image; *PTEN*, phosphatase and tensin homolog.

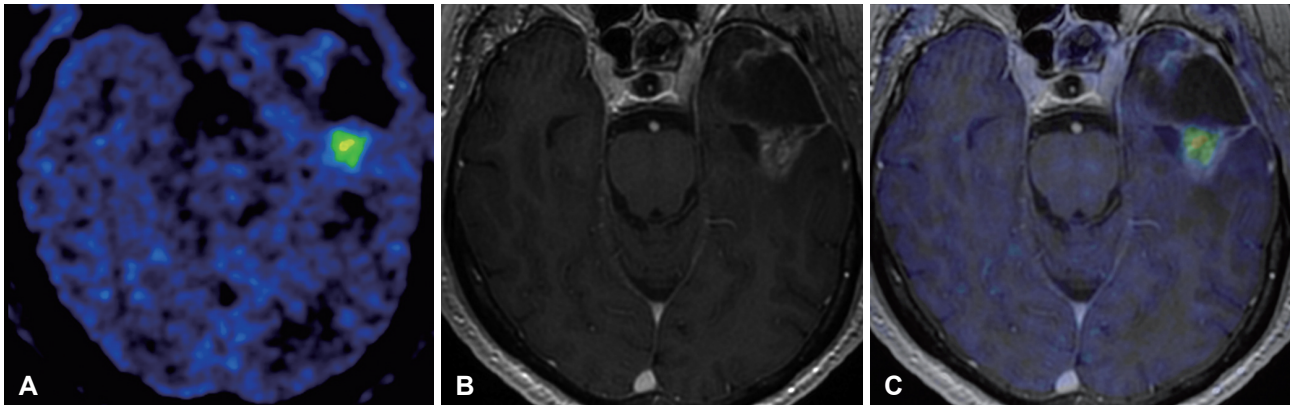

Fig. 6. Single modality FMISO PET/MR imaging in a 65-year-old man with recurrent left temporal lobe WHO grade III anaplastic astrocytoma. Simultaneously obtained, axial FMISO PET (A), post contrast T1-weighted (B), and fused T1 post contrast FMISO (C) PET/MR demonstrates recurrence of disease evidenced by contrast enhancing focus bordering the posterior margin of an anterior left temporal lobe resection cavity. This region demonstrates increased FMISO uptake. FMISO, ^{18}F-flouromisoidazole; MR, magnetic resonance; PET, positron emission tomography; WHO, World Health Organization.

Table 2. Imaging methods and the major utility in brain tumor imaging

Imaging technique	Major utility in brain tumor imaging
CT	Mass effect, herniation, hydrocephalus, hemorrhage, calcifications
Pre and post-contrast T1	Enhancement characteristics, necrosis, extent of the enhancing portion of the tumor
T2/T2 FLAIR	Peri-tumoral edema (vasogenic and infiltrative), non-enhancing tumor
T2* susceptibility sequence (SWI)	Blood products, calcifications, radiation induced chronic micro-hemorrhages
DWI/ADC	Reduced in highly cellular portions of tumor, post-operative injury
DTI	Tractography for surgical planning/navigation
Perfusion (generally DSC)	Tumor/tissue vascularity
MR spectroscopy	Metabolic profile
fMRI	Pre-operative functional mapping, research into treatment effects
PET/MR	Potential new radiotracers

ADC, apparent diffusion coefficient; CT, computed tomography; DSC, dynamic susceptibility contrast-enhanced; DTI, diffusion tensor imaging; DWI, diffusion weighted imaging; FLAIR, fluid attenuated inversion recovery; fMRI, functional magnetic resonance imaging; PET, positron emission tomography; SWI, susceptibility weighted imaging

With regards to gliomas, lower ADC values have been reported in higher-grade gliomas than lower-grade gliomas and lower ADC values have been reported to have a poorer prognosis independent of tumor grade [103-105]. Similarly in primary CNS lymphoma lower ADC values have been reported to be associated with a poorer prognosis [99,106]. ADC values have also been reported to be higher in the vasogenic peritumoral edema T2/FLAIR abnormality surrounding metastases than in the more cellular infiltrative peritumoral edema T2/FLAIR abnormality seen in glioblastoma although this has not been found consistently in all studies [105,107-109].

In the immediate post-operative setting it is common to see small areas of reduced diffusion at the surgical bed indicating areas of devitalized tumor tissue or ischemic brain tissue during surgery [110]. These small areas of postoperative injury may be caused by a variety of reasons including direct surgical trauma, retraction, vascular injury, and devascularization. The clinical implication of this finding is in the knowledge that these areas may be expected to develop contrast enhancement and normalization of ADC on subsequent imaging as a cerebral infarction would be expected to and that the contrast enhancement should not be mistaken for tumor progression [110].

DWI and quantitative ADC measurements may also be helpful in the setting of pseudo-response and pseudo-progression. In pseudo-response to bevacizumab, DWI may be useful to demonstrate persistent or progressive tumor despite the lack of contrast enhancement caused by the antiangiogenic effects of bevacizumab [111]. Histogram analysis of ADC maps has also been used to demonstrate poorer survival in patients with recurrent glioblastoma being treated with bevacizumab [112]. In the setting of possible pseudo-progression DWI/ADC may potentially offer some utility. Lower ADC values have been reported in tumor progression than in pseudo-progression, presumably due to the cellular nature of true tumor and the edema associated with the inflammatory response in pseudo-progression [113,114].

Diffusion-tensor imaging (DTI) involves more directions of interrogation than standard DWI but provides additional

parameters and abilities over DWI. DTI provides information on anisotropic diffusion characterized by eigenvectors (direction) and eigenvalues (magnitude), which can be used to derive numerous parameters. DTI and other similar advanced predominately research techniques such as diffusion-spectrum imaging, diffusion-kurtosis imaging, tract-density imaging, and numerous others provide additional insight beyond DWI into the microstructure and integrity of the white matter. Fractional anisotropy (FA), mean diffusivity, track density, neuronal density and multiple other measures derived from these techniques offer additional means to study brain tumors and the effects of treatment. DTI is currently most relevant clinically as DTI-tractography where white matter fiber tracts can be displayed three-dimensionally for navigational purposes (Fig. 1-3) [65,115]. Tractography of the corticospinal tract is routinely displayed superimposed on high-resolution 3D T2-weighted and post-gadolinium SPGR images for intraoperative navigational purposes in order to avoid injuring the corticospinal tracts. FA derived from DTI is a measure of the directional nature of water diffusivity and has been used as a marker of white matter integrity in multiple conditions. FA has been shown to decrease in normal appearing white matter following radiation therapy and thus offers insight into the effects of radiation damage to the brains of brain tumors patients [116,117]. FA has also been reported to be increased in the infiltrative peritumoral edema surrounding high-grade gliomas as compared to the vasogenic edema surrounding metastases, presumably due to the more ordered nature of the more cellular edema associated with gliomas [79].

PERFUSION IMAGING

The two main methods of MR perfusion imaging include T2*-weighted dynamic susceptibility contrast-enhanced (DSC) perfusion and T1-weighted dynamic contrast-enhanced (DCE) perfusion. DSC is a first-pass bolus tracking blood volume technique and DCE is a steady state permeability technique. Both can be used to derive multiple perfusion parameters such as cerebral blood volume (CBV) and endothelial transfer coefficient (K^{trans}). Arterial spin labeling is a non-contrast perfusion technique, which may prove useful in the future but has not yet been as well studied or established in the evaluation of brain tumors. The complexity of perfusion data sets, which consist of hemodynamic parameters calculated on a pixel-by-pixel basis, and the heterogeneity of brain tumors make reliable interpretation of these studies challenging.

Relative cerebral blood volume (rCBV), which is the calculated CBV relative to the contralateral side, is the most widely used parameter derived from DSC and is considered a marker of angiogenesis. rCBV may be helpful in distinguishing high-grade from low-grade gliomas as high-grade gliomas have been found to have higher rCBV than low-grade gliomas, however this should be used with caution as oligodendrogliomas can have high rCBVs [118-122]. Metastases can have high rCBV similar to high-grade gliomas however they tend to have very leaky capillaries in the tumors and as a result may demonstrate leakage of contrast in the bolus phase and as a result the signal intensity curve may not return to baseline (Fig. 4) [1,82]. A similar pattern resulting from highly leaky capillaries has been seen with choroid plexus tumors [1,123]. rCBV has also been reported to more elevated in the infiltrate more cellular peritumoral T2/FLAIR abnormality surrounding high-grade gliomas as compared to the vasogenic peritumoral T2/FLAIR abnormality surrounding metastases [80]. DSC may also be useful in distinguishing tumefactive demyelinating lesions from high-grade gliomas as tumefactive demyelinating lesions generally have a lower rCBV [83]. DSC may also be helpful in the ongoing evaluation of patients with known brain tumors, as recurrent or residual tumor has been shown to have higher rCBV than pseudo-progression or radiation necrosis in the setting of gliomas and metastases [47,124,125].

The main metric derived from DCE perfusion MRI is K^{trans}. considered a measure of microvascular permeability. DCE perfusion imaging is less frequently used than DSC but offers some theoretical advantages including better spatial resolution and less susceptibility artifact [1]. DCE may potentially be used to distinguish low-grade from high-grade gliomas with higher K^{trans} presumably due to greater capillary permeability seen in higher-grade gliomas [126-129]. DCE has not been as extensively studied in the evaluation of treatment response as DSC but has been reported to be able to distinguish recurrent or progressive tumor from pseudo-progression using the maximum slope of initial enhancement [130]. DCE perfusion imaging offers potential advantage over DSC perfusion imaging due to its resilience to susceptibility artifact, higher spatial resolution, and 3D acquisition.

MR SPECTROSCOPY

MRS provides insight into the metabolic profile of interrogated tissue. The most recognizable metabolites on ^{1}H-MRS, which are of primary interest in the evaluation of brain tumors, include N-acetylaspartate (NAA) at approximately 2.0 parts per million (ppm), creatine (Cr) at approximately 3.0 ppm, and choline (Cho) at approximately 3.2 ppm [131]. NAA is considered a neuronal marker, Cr a marker for cellular metabolism, and Cho a marker for cell membrane turnover. Additional metabolites of interest include lipid and lactate peaks at approximately 1.3 ppm and myo-inositol at approximately 3.5 ppm. Lipids and lactate are considered markers of necrosis and hy-

poxia, respectively, and myo-inositol is considered to be related to astrocytic integrity and regulation of brain osmosis [131-134].

The MRS profile of gliomas is generally considered elevated Cho and decreased NAA [135-137]. Cho is not a marker of tumor but reflects increase in cell membrane turnover and NAA represents a neuronal marker. Absolute heights of the MRS peaks are generally not used and the metabolic peaks are generally analyzed as ratios including Cho-NAA and Cho-Cr (Fig. 3). MRS can potentially be used to differentiate high-grade gliomas from low-grade gliomas as high-grade gliomas have been found to have higher Cho-NAA and Cho-Cr ratios than lower-grade gliomas [137,138]. Furthermore, an elevated myo-inositol/Cr ratio (myo-inositol is best identified with a short echo time of 35 ms) is associated with lower-grade gliomas [132]. Elevated Cho-NAA and Cho-Cr ratios in the peritumoral T2/FLAIR adjacent to an enhancing lesion can also be used to distinguish the peritumoral infiltrative edema of high-grade gliomas, which has elevated Cho-NAA and Cho-Cr ratios reflecting the cellular nature of the signal abnormality, from the peritumoral vasogenic edema surrounding metastases [80,139]. MRS may also useful in the ongoing evaluation of patients with known brain tumors. In the situation of possible pseudo-progression or radiation necrosis, elevated Cho-NAA or Cho-Cr have been reported to be suggestive of tumor while non-elevated ratios are suggestive of pseudo-progression or radiation necrosis, however, in practice this may be a challenging distinction to make on MRS [140-144].

The lipid and lactate peaks overlap on standard MRS and may be interpreted as one metabolite even through they provide different and unique information or potentially cancel each other's signal on lactate-edited MRS is a technique which can reliable separate the lactate doublet peak from lipid peaks [145]. Lactate-edited MRS is of interest as lactate reflecting hypoxia and anaerobic metabolism is encountered in high and low-grade gliomas whereas lipid, representing necrosis is seen in high-grade gliomas [146]. Higher levels of lactate and lipids in patients with glioblastoma have also been associated with worse overall survival [147].

A related emerging method currently confined to research use is hyperpolarized ^{13}C MR. Hyperpolarized ^{13}C agents have a dramatically increased signal, which provides the opportunity to follow a substance such as pyruvate through its biochemical pathways as it is converted to alanine, lactate, and bicarbonate [148,149]. In animal brain tumor models hyperpolarized ^{13}C labeled lactate has been demonstrated within tumors with a reduction in lactate following treatment with temozolamide [150]. Hyperpolarized ^{13}C MRS has also been shown to be able to detect *IDH1* mutation status by analyzing the metabolites of hyperpolarized ^{13}C alpha ketoglutarate in an animal tumor model [151].

FUNCTIONAL MRI

Functional MRI (fMRI) utilizes relative changes in the blood oxygen level dependent (BOLD) signal to infer brain activity [152]. fMRI can be either task-based where the sequence is performed during the performance of a task or during exposure to a stimulus, or non-task based where the sequence is performed at rest and termed resting-state fMRI (RS-fMRI). RS-fMRI uses spontaneous low frequency fluctuations (<0.1 Hz) in the BOLD signal to pick out areas of correlation and anti-correlation, which form the basis for defining resting-state networks, the most widely studied of which is the default mode network [152-155]. Vascular tumors can potentially affect the BOLD signal, however, both task based and RS-fMRI have been effectively applied in patients with brain tumors.

Task based fMRI can be used for pre-operative localization of eloquent cortex with identification of language and somatomotor function with similar accuracy to more invasive techniques (Fig. 5) [156-158]. Task based fMRI has thus been used for preoperative planning in order to identify the relationship of eloquent functional cortex to brain tumors [159]. The distance from the tumor to functional area depicted on task-based fMRI has been shown to be related to the degree of postoperative loss of function with a small margin (<1 cm) predicting a poorer neurologic outcome [159].

RS-fMRI has also been used to identify eloquent cortex as part of pre-surgical planning in brain tumor patients although the experience is more limited [160]. RS-fMRI carries some distinct advantages over task based fMRI including not having to administer a paradigm, the ability to study patients who may not be able cooperate with a paradigm (children, patients with altered mental status, etc.), and the ability to detect many networks retrospectively from one sequence. Although the experience is more limited, several studies have demonstrated the ability to localize somatosensory cortex in relationship to brain tumors [161,162]. RS-fMRI offers the ability to study functional connectivity of the brain and is thus a potentially powerful sequence for studying the healthy and diseased brain. RS-fMRI may potentially be used in the future to study not only the effects of brain tumors on the brain, but also the effects of treatment. To date there have been several small studies which have demonstrated decreased functional connectivity in resting state networks in brain tumor patients but this will likely be an area of active research in the future [163-165].

PET MRI

Integrated PET/MRI systems offers the ability to perform state of the art structural MR imaging simultaneously with physiologic PET imaging and is an area of active research

[166,167]. The ideal radiotracer has robust uptake in the targeted lesion with minimal physiological uptake in normal background tissues. The high glucose metabolic activity of the brain and gliomas limits the utility of ^{18}F-fluorodeoxyglucose PET imaging due to the poor tumor to background contrast [168,169].

New PET tracers however may offer additional insight into brain tumor physiology. The amino acid PET tracers ^{11}C-methionine (MET) and ^{18}F-flouroethyltyrosine (FET) demonstrate increased uptake in gliomas as compared to normal brain and elevated uptake in high-grade gliomas as compared to low-grade gliomas [170-173]. Furthermore these agents may offer prognostic information as poorer survival has been associated in low-grade glioma patients with elevated MET [170]. These amino acid PET tracers may also be useful for distinguishing recurrent/progressive tumor from pseudo-progression/treatment effect with both relative elevated MET and FET suggesting tumor [174,175]. However, the clinical utility of MET is limited by it's short half-life of 20.3 minutes and need for an onsite cyclotron. ^{18}F-flouro-L-dopa (FDOPA) is additional marker of amino acid synthesis. FDOPA uptake has been shown to correlate with regions of high proliferation and demonstrate uptake in low and high-grade gliomas [176,177]. FDOPA has also been reported to be elevated in recurrent/progressive tumor as compared to radiation necrosis [176,178].

^{18}F-flouromisoidazole (FMISO) PET is a non-invasive method that can physiologically estimate tissue hypoxia (Fig. 6) [179-183]. Several studies have validated FMISO uptake as a robust measure of tissue hypoxia, and established methodology for FMISO PET imaging [179-183]. A preliminary study of 22 participants with glioblastoma demonstrated an association with both the pre-radiation volume and degree of tumor hypoxia measured by FMISO PET and a shorter time to tumor progression and survival [183]. Consequently, knowledge of the amount and distribution of tumor hypoxia may provide prognostic information as well as useful information to guide therapy for patients with glioblastoma. The use of hypoxia imaging markers could serve as early biomarkers of radiation resistant areas and provide insight into patient prognosis prior to anti-angiogenic therapy.

CONCLUSION

The imaging and clinical management of patients with brain tumor continue to evolve over time and now heavily relies on physiologic imaging in addition to high-resolution structural imaging. As our understanding of the biology of brain tumors and our imaging abilities increase there is a great opportunity to positively impact the care of brain tumor patients. Ongoing research is required to understand the interactions of our modern neuroimaging techniques with advancements in tumor genetics, therapeutics, and neuroscience. Many of the established and developing imaging techniques discussed in this review may offer additional insight into genetic, prognostic, and predictive information that may be further elucidated in the future. The current state of brain tumor imaging contributes greatly to improving preoperative diagnosis, predicting tumor grading and patient prognosis, planning surgery and radiation therapy, and assessing treatment response. Imaging remains a powerful noninvasive tool to positively impact the management of patients with brain tumor.

Conflicts of Interest

The authors have no financial conflicts of interest.

Acknowledgments

MCM was supported by an NIH T32 training grant (5T32EB001631-10).

REFERENCES

1. Cha S. Update on brain tumor imaging: from anatomy to physiology. AJNR Am J Neuroradiol 2006;27:475-87.
2. Belden CJ, Valdes PA, Ran C, et al. Genetics of glioblastoma: a window into its imaging and histopathologic variability. Radiographics 2011; 31:1717-40.
3. Bangiyev L, Rossi Espagnet MC, Young R, et al. Adult brain tumor imaging: state of the art. Semin Roentgenol 2014;49:39-52.
4. Louis DN, Ohgaki H, Wiestler OD, et al. The 2007 WHO classification of tumours of the central nervous system. Acta Neuropathol 2007;114:97-109.
5. Zulch KJ. Histological typing of tumours of the central nervous system. Geneva: World Health Organization; 1979.
6. Kleihues P, Sobin LH. World Health Organization classification of tumors. Cancer 2000;88:2887.
7. Kleihues P, Burger PC, Scheithauer BW. The new WHO classification of brain tumours. Brain Pathol 1993;3:255-68.
8. Gupta K, Salunke P. Molecular markers of glioma: an update on recent progress and perspectives. J Cancer Res Clin Oncol 2012;138:1971-81.
9. Cancer Genome Atlas Research Network. Comprehensive genomic characterization defines human glioblastoma genes and core pathways. Nature 2008;455:1061-8.
10. Shiraishi S, Tada K, Nakamura H, et al. Influence of p53 mutations on prognosis of patients with glioblastoma. Cancer 2002;95:249-57.
11. Furnari FB, Fenton T, Bachoo RM, et al. Malignant astrocytic glioma: genetics, biology, and paths to treatment. Genes Dev 2007;21:2683-710.
12. Yip S, Iafrate AJ, Louis DN. Molecular diagnostic testing in malignant gliomas: a practical update on predictive markers. J Neuropathol Exp Neurol 2008;67:1-15.
13. Shinojima N, Tada K, Shiraishi S, et al. Prognostic value of epidermal growth factor receptor in patients with glioblastoma multiforme. Cancer Res 2003;63:6962-70.
14. Huncharek M, Kupelnick B. Epidermal growth factor receptor gene amplification as a prognostic marker in glioblastoma multiforme: results of a meta-analysis. Oncol Res 2000;12:107-12.
15. Mellinghoff IK, Wang MY, Vivanco I, et al. Molecular determinants of the response of glioblastomas to EGFR kinase inhibitors. N Engl J Med 2005;353:2012-24.
16. Ohgaki H, Kleihues P. Genetic alterations and signaling pathways in the evolution of gliomas. Cancer Sci 2009;100:2235-41.
17. Horbinski C, Miller CR, Perry A. Gone FISHing: clinical lessons learned in brain tumor molecular diagnostics over the last decade. Brain Pathol

2011;21:57-73.
18. Diehn M, Nardini C, Wang DS, et al. Identification of noninvasive imaging surrogates for brain tumor gene-expression modules. Proc Natl Acad Sci U S A 2008;105:5213-8.
19. Young RJ, Gupta A, Shah AD, et al. Potential role of preoperative conventional MRI including diffusion measurements in assessing epidermal growth factor receptor gene amplification status in patients with glioblastoma. AJNR Am J Neuroradiol 2013;34:2271-7.
20. Aghi M, Gaviani P, Henson JW, Batchelor TT, Louis DN, Barker FG 2nd. Magnetic resonance imaging characteristics predict epidermal growth factor receptor amplification status in glioblastoma. Clin Cancer Res 2005; 11(24 Pt 1):8600-5.
21. Ryoo I, Choi SH, Kim JH, et al. Cerebral blood volume calculated by dynamic susceptibility contrast-enhanced perfusion MR imaging: preliminary correlation study with glioblastoma genetic profiles. PLoS One 2013;8:e71704.
22. Hartmann C, Meyer J, Balss J, et al. Type and frequency of IDH1 and IDH2 mutations are related to astrocytic and oligodendroglial differentiation and age: a study of 1,010 diffuse gliomas. Acta Neuropathol 2009; 118:469-74.
23. Ichimura K, Pearson DM, Kocialkowski S, et al. IDH1 mutations are present in the majority of common adult gliomas but rare in primary glioblastomas. Neuro Oncol 2009;11:341-7.
24. Yan H, Parsons DW, Jin G, et al. IDH1 and IDH2 mutations in gliomas. N Engl J Med 2009;360:765-73.
25. van den Bent MJ, Dubbink HJ, Marie Y, et al. IDH1 and IDH2 mutations are prognostic but not predictive for outcome in anaplastic oligodendroglial tumors: a report of the European Organization for Research and Treatment of Cancer Brain Tumor Group. Clin Cancer Res 2010;16: 1597-604.
26. Wick W, Hartmann C, Engel C, et al. NOA-04 randomized phase III trial of sequential radiochemotherapy of anaplastic glioma with procarbazine, lomustine, and vincristine or temozolomide. J Clin Oncol 2009;27:5874-80.
27. Carrillo JA, Lai A, Nghiemphu PL, et al. Relationship between tumor enhancement, edema, IDH1 mutational status, MGMT promoter methylation, and survival in glioblastoma. AJNR Am J Neuroradiol 2012;33: 1349-55.
28. Seiz M, Tuettenberg J, Meyer J, et al. Detection of IDH1 mutations in gliomatosis cerebri, but only in tumors with additional solid component: evidence for molecular subtypes. Acta Neuropathol 2010;120:261-7.
29. Choi C, Ganji SK, DeBerardinis RJ, et al. 2-hydroxyglutarate detection by magnetic resonance spectroscopy in IDH-mutated patients with gliomas. Nat Med 2012;18:624-9.
30. Riemenschneider MJ, Jeuken JW, Wesseling P, Reifenberger G. Molecular diagnostics of gliomas: state of the art. Acta Neuropathol 2010;120: 567-84.
31. Labussière M, Idbaih A, Wang XW, et al. All the 1p19q codeleted gliomas are mutated on IDH1 or IDH2. Neurology 2010;74:1886-90.
32. Cairncross JG, Ueki K, Zlatescu MC, et al. Specific genetic predictors of chemotherapeutic response and survival in patients with anaplastic oligodendrogliomas. J Natl Cancer Inst 1998;90:1473-9.
33. van den Bent MJ, Carpentier AF, Brandes AA, et al. Adjuvant procarbazine, lomustine, and vincristine improves progression-free survival but not overall survival in newly diagnosed anaplastic oligodendrogliomas and oligoastrocytomas: a randomized European Organisation for Research and Treatment of Cancer phase III trial. J Clin Oncol 2006;24: 2715-22.
34. Trost D, Ehrler M, Fimmers R, et al. Identification of genomic aberrations associated with shorter overall survival in patients with oligodendroglial tumors. Int J Cancer 2007;120:2368-76.
35. Cairncross G, Wang M, Shaw E, et al. Phase III trial of chemoradiotherapy for anaplastic oligodendroglioma: long-term results of RTOG 9402. J Clin Oncol 2013;31:337-43.
36. Weller M, Pfister SM, Wick W, Hegi ME, Reifenberger G, Stupp R. Molecular neuro-oncology in clinical practice: a new horizon. Lancet Oncol 2013;14:e370-9.
37. Idbaih A, Marie Y, Pierron G, et al. Two types of chromosome 1p losses with opposite significance in gliomas. Ann Neurol 2005;58:483-7.
38. Jenkinson MD, du Plessis DG, Smith TS, Joyce KA, Warnke PC, Walker C. Histological growth patterns and genotype in oligodendroglial tumours: correlation with MRI features. Brain 2006;129(Pt 7):1884-91.
39. Whitmore RG, Krejza J, Kapoor GS, et al. Prediction of oligodendroglial tumor subtype and grade using perfusion weighted magnetic resonance imaging. J Neurosurg 2007;107:600-9.
40. Kapoor GS, Gocke TA, Chawla S, et al. Magnetic resonance perfusion-weighted imaging defines angiogenic subtypes of oligodendroglioma according to 1p19q and EGFR status. J Neurooncol 2009;92:373-86.
41. Nakagawachi T, Soejima H, Urano T, et al. Silencing effect of CpG island hypermethylation and histone modifications on O6-methylguanine-DNA methyltransferase (MGMT) gene expression in human cancer. Oncogene 2003;22:8835-44.
42. Esteller M, Garcia-Foncillas J, Andion E, et al. Inactivation of the DNA-repair gene MGMT and the clinical response of gliomas to alkylating agents. N Engl J Med 2000;343:1350-4.
43. Hegi ME, Diserens AC, Gorlia T, et al. MGMT gene silencing and benefit from temozolomide in glioblastoma. N Engl J Med 2005;352:997-1003.
44. Stupp R, Mason WP, van den Bent MJ, et al. Radiotherapy plus concomitant and adjuvant temozolomide for glioblastoma. N Engl J Med 2005;352:987-96.
45. Gorlia T, van den Bent MJ, Hegi ME, et al. Nomograms for predicting survival of patients with newly diagnosed glioblastoma: prognostic factor analysis of EORTC and NCIC trial 26981-22981/CE.3. Lancet Oncol 2008;9:29-38.
46. Brandes AA, Franceschi E, Tosoni A, et al. MGMT promoter methylation status can predict the incidence and outcome of pseudoprogression after concomitant radiochemotherapy in newly diagnosed glioblastoma patients. J Clin Oncol 2008;26:2192-7.
47. Kong DS, Kim ST, Kim EH, et al. Diagnostic dilemma of pseudoprogression in the treatment of newly diagnosed glioblastomas: the role of assessing relative cerebral blood flow volume and oxygen-6-methylguanine-DNA methyltransferase promoter methylation status. AJNR Am J Neuroradiol 2011;32:382-7.
48. von Deimling A, Korshunov A, Hartmann C. The next generation of glioma biomarkers: MGMT methylation, BRAF fusions and IDH1 mutations. Brain Pathol 2011;21:74-87.
49. Davies H, Bignell GR, Cox C, et al. Mutations of the BRAF gene in human cancer. Nature 2002;417:949-54.
50. Jones DT, Kocialkowski S, Liu L, Pearson DM, Ichimura K, Collins VP. Oncogenic RAF1 rearrangement and a novel BRAF mutation as alternatives to KIAA1549:BRAF fusion in activating the MAPK pathway in pilocytic astrocytoma. Oncogene 2009;28:2119-23.
51. Jones DT, Kocialkowski S, Liu L, et al. Tandem duplication producing a novel oncogenic BRAF fusion gene defines the majority of pilocytic astrocytomas. Cancer Res 2008;68:8673-7.
52. Horbinski C, Nikiforova MN, Hagenkord JM, Hamilton RL, Pollack IF. Interplay among BRAF, p16, p53, and MIB1 in pediatric low-grade gliomas. Neuro Oncol 2012;14:777-89.
53. Heaphy CM, de Wilde RF, Jiao Y, et al. Altered telomeres in tumors with ATRX and DAXX mutations. Science 2011;333:425.
54. Lovejoy CA, Li W, Reisenweber S, et al. Loss of ATRX, genome instability, and an altered DNA damage response are hallmarks of the alternative lengthening of telomeres pathway. PLoS Genet 2012;8:e1002772.
55. Jiao Y, Killela PJ, Reitman ZJ, et al. Frequent ATRX, CIC, FUBP1 and IDH1 mutations refine the classification of malignant gliomas. Oncotarget 2012;3:709-22.
56. Liu XY, Gerges N, Korshunov A, et al. Frequent ATRX mutations and loss of expression in adult diffuse astrocytic tumors carrying IDH1/IDH2 and TP53 mutations. Acta Neuropathol 2012;124:615-25.

57. Khuong-Quang DA, Buczkowicz P, Rakopoulos P, et al. K27M mutation in histone H3.3 defines clinically and biologically distinct subgroups of pediatric diffuse intrinsic pontine gliomas. Acta Neuropathol 2012; 124:439-47.
58. Schwartzentruber J, Korshunov A, Liu XY, et al. Driver mutations in histone H3.3 and chromatin remodelling genes in paediatric glioblastoma. Nature 2012;482:226-31.
59. Wiestler B, Capper D, Holland-Letz T, et al. ATRX loss refines the classification of anaplastic gliomas and identifies a subgroup of IDH mutant astrocytic tumors with better prognosis. Acta Neuropathol 2013;126:443-51.
60. Wu G, Broniscer A, McEachron TA, et al. Somatic histone H3 alterations in pediatric diffuse intrinsic pontine gliomas and non-brainstem glioblastomas. Nat Genet 2012;44:251-3.
61. Sturm D, Witt H, Hovestadt V, et al. Hotspot mutations in H3F3A and IDH1 define distinct epigenetic and biological subgroups of glioblastoma. Cancer Cell 2012;22:425-37.
62. Lee YY, Van Tassel P. Intracranial oligodendrogliomas: imaging findings in 35 untreated cases. AJR Am J Roentgenol 1989;152:361-9.
63. Eskandary H, Sabba M, Khajehpour F, Eskandari M. Incidental findings in brain computed tomography scans of 3000 head trauma patients. Surg Neurol 2005;63:550-3; discussion 553.
64. Gumprecht HK, Widenka DC, Lumenta CB. BrainLab VectorVision Neuronavigation System: technology and clinical experiences in 131 cases. Neurosurgery 1999;44:97-104; discussion 104-5.
65. Elhawary H, Liu H, Patel P, et al. Intraoperative real-time querying of white matter tracts during frameless stereotactic neuronavigation. Neurosurgery 2011;68:506-16; discussion 516.
66. Zhang B, MacFadden D, Damyanovich AZ, et al. Development of a geometrically accurate imaging protocol at 3 Tesla MRI for stereotactic radiosurgery treatment planning. Phys Med Biol 2010;55:6601-15.
67. Saconn PA, Shaw EG, Chan MD, et al. Use of 3.0-T MRI for stereotactic radiosurgery planning for treatment of brain metastases: a single-institution retrospective review. Int J Radiat Oncol Biol Phys 2010;78:1142-6.
68. Haacke EM. Susceptibility weighted imaging (SWI). Z Med Phys 2006; 16:237.
69. Haacke EM, Mittal S, Wu Z, Neelavalli J, Cheng YC. Susceptibility-weighted imaging: technical aspects and clinical applications, part 1. AJNR Am J Neuroradiol 2009;30:19-30.
70. Bian W, Hess CP, Chang SM, Nelson SJ, Lupo JM. Susceptibility-weighted MR imaging of radiation therapy-induced cerebral microbleeds in patients with glioma: a comparison between 3T and 7T. Neuroradiology 2014;56:91-6.
71. Borja MJ, Plaza MJ, Altman N, Saigal G. Conventional and advanced MRI features of pediatric intracranial tumors: supratentorial tumors. AJR Am J Roentgenol 2013;200:W483-503.
72. Sze G, Milano E, Johnson C, Heier L. Detection of brain metastases: comparison of contrast-enhanced MR with unenhanced MR and enhanced CT. AJNR Am J Neuroradiol 1990;11:785-91.
73. White ML, Zhang Y, Kirby P, Ryken TC. Can tumor contrast enhancement be used as a criterion for differentiating tumor grades of oligodendrogliomas? AJNR Am J Neuroradiol 2005;26:784-90.
74. Ginsberg LE, Fuller GN, Hashmi M, Leeds NE, Schomer DF. The significance of lack of MR contrast enhancement of supratentorial brain tumors in adults: histopathological evaluation of a series. Surg Neurol 1998;49:436-40.
75. Garzón B, Emblem KE, Mouridsen K, et al. Multiparametric analysis of magnetic resonance images for glioma grading and patient survival time prediction. Acta Radiol 2011;52:1052-60.
76. Koeller KK, Rushing EJ. From the archives of the AFIP: pilocytic astrocytoma: radiologic-pathologic correlation. Radiographics 2004;24:1693-708.
77. Lee YY, Van Tassel P, Bruner JM, Moser RP, Share JC. Juvenile pilocytic astrocytomas: CT and MR characteristics. AJR Am J Roentgenol 1989; 152:1263-70.
78. Klatzo I. Presidental address. Neuropathological aspects of brain edema. J Neuropathol Exp Neurol 1967;26:1-14.
79. Lu S, Ahn D, Johnson G, Cha S. Peritumoral diffusion tensor imaging of high-grade gliomas and metastatic brain tumors. AJNR Am J Neuroradiol 2003;24:937-41.
80. Law M, Cha S, Knopp EA, Johnson G, Arnett J, Litt AW. High-grade gliomas and solitary metastases: differentiation by using perfusion and proton spectroscopic MR imaging. Radiology 2002;222:715-21.
81. Barajas RF Jr, Hess CP, Phillips JJ, et al. Super-resolution track density imaging of glioblastoma: histopathologic correlation. AJNR Am J Neuroradiol 2013;34:1319-25.
82. Cha S, Lupo JM, Chen MH, et al. Differentiation of glioblastoma multiforme and single brain metastasis by peak height and percentage of signal intensity recovery derived from dynamic susceptibility-weighted contrast-enhanced perfusion MR imaging. AJNR Am J Neuroradiol 2007; 28:1078-84.
83. Cha S, Pierce S, Knopp EA, et al. Dynamic contrast-enhanced T2*-weighted MR imaging of tumefactive demyelinating lesions. AJNR Am J Neuroradiol 2001;22:1109-16.
84. Stadnik TW, Chaskis C, Michotte A, et al. Diffusion-weighted MR imaging of intracerebral masses: comparison with conventional MR imaging and histologic findings. AJNR Am J Neuroradiol 2001;22:969-76.
85. Tung GA, Evangelista P, Rogg JM, Duncan JA 3rd. Diffusion-weighted MR imaging of rim-enhancing brain masses: is markedly decreased water diffusion specific for brain abscess? AJR Am J Roentgenol 2001;177: 709-12.
86. Ebisu T, Tanaka C, Umeda M, et al. Discrimination of brain abscess from necrotic or cystic tumors by diffusion-weighted echo planar imaging. Magn Reson Imaging 1996;14:1113-6.
87. Desprechins B, Stadnik T, Koerts G, Shabana W, Breucq C, Osteaux M. Use of diffusion-weighted MR imaging in differential diagnosis between intracerebral necrotic tumors and cerebral abscesses. AJNR Am J Neuroradiol 1999;20:1252-7.
88. Raz E, Zagzag D, Saba L, et al. Cyst with a mural nodule tumor of the brain. Cancer Imaging 2012;12:237-44.
89. Kondziolka D, Bernstein M, Resch L, et al. Significance of hemorrhage into brain tumors: clinicopathological study. J Neurosurg 1987;67:852-7.
90. Rees JH, Smirniotopoulos JG, Jones RV, Wong K. Glioblastoma multiforme: radiologic-pathologic correlation. Radiographics 1996;16:1413-38; quiz 1462-3.
91. Wen PY, Macdonald DR, Reardon DA, et al. Updated response assessment criteria for high-grade gliomas: response assessment in neuro-oncology working group. J Clin Oncol 2010;28:1963-72.
92. Batchelor TT, Sorensen AG, di Tomaso E, et al. AZD2171, a pan-VEGF receptor tyrosine kinase inhibitor, normalizes tumor vasculature and alleviates edema in glioblastoma patients. Cancer Cell 2007;11:83-95.
93. Pope WB, Lai A, Nghiemphu P, Mischel P, Cloughesy TF. MRI in patients with high-grade gliomas treated with bevacizumab and chemotherapy. Neurology 2006;66:1258-60.
94. Thompson EM, Frenkel EP, Neuwelt EA. The paradoxical effect of bevacizumab in the therapy of malignant gliomas. Neurology 2011;76:87-93.
95. Taal W, Brandsma D, de Bruin HG, et al. Incidence of early pseudo-progression in a cohort of malignant glioma patients treated with chemoirradiation with temozolomide. Cancer 2008;113:405-10.
96. Brandsma D, Stalpers L, Taal W, Sminia P, van den Bent MJ. Clinical features, mechanisms, and management of pseudoprogression in malignant gliomas. Lancet Oncol 2008;9:453-61.
97. Gaensler EH, Dillon WP, Edwards MS, Larson DA, Rosenau W, Wilson CB. Radiation-induced telangiectasia in the brain simulates cryptic vascular malformations at MR imaging. Radiology 1994;193:629-36.
98. Lupo JM, Chuang CF, Chang SM, et al. 7-Tesla susceptibility-weighted imaging to assess the effects of radiotherapy on normal-appearing brain in patients with glioma. Int J Radiat Oncol Biol Phys 2012;82:e493-500.
99. Barajas RF Jr, Rubenstein JL, Chang JS, Hwang J, Cha S. Diffusion-weight-

ed MR imaging derived apparent diffusion coefficient is predictive of clinical outcome in primary central nervous system lymphoma. AJNR Am J Neuroradiol 2010;31:60-6.
100. Guo AC, Cummings TJ, Dash RC, Provenzale JM. Lymphomas and high-grade astrocytomas: comparison of water diffusibility and histologic characteristics. Radiology 2002;224:177-83.
101. Herneth AM, Guccione S, Bednarski M. Apparent diffusion coefficient: a quantitative parameter for in vivo tumor characterization. Eur J Radiol 2003;45:208-13.
102. Rumboldt Z, Camacho DL, Lake D, Welsh CT, Castillo M. Apparent diffusion coefficients for differentiation of cerebellar tumors in children. AJNR Am J Neuroradiol 2006;27:1362-9.
103. Hilario A, Sepulveda JM, Perez-Nuñez A, et al. A prognostic model based on preoperative MRI predicts overall survival in patients with diffuse gliomas. AJNR Am J Neuroradiol 2014;35:1096-102.
104. Bulakbasi N, Guvenc I, Onguru O, Erdogan E, Tayfun C, Ucoz T. The added value of the apparent diffusion coefficient calculation to magnetic resonance imaging in the differentiation and grading of malignant brain tumors. J Comput Assist Tomogr 2004;28:735-46.
105. Kono K, Inoue Y, Nakayama K, et al. The role of diffusion-weighted imaging in patients with brain tumors. AJNR Am J Neuroradiol 2001;22: 1081-8.
106. Valles FE, Perez-Valles CL, Regalado S, Barajas RF, Rubenstein JL, Cha S. Combined diffusion and perfusion MR imaging as biomarkers of prognosis in immunocompetent patients with primary central nervous system lymphoma. AJNR Am J Neuroradiol 2013;34:35-40.
107. Lee EJ, terBrugge K, Mikulis D, et al. Diagnostic value of peritumoral minimum apparent diffusion coefficient for differentiation of glioblastoma multiforme from solitary metastatic lesions. AJR Am J Roentgenol 2011;196:71-6.
108. Oh J, Cha S, Aiken AH, et al. Quantitative apparent diffusion coefficients and T2 relaxation times in characterizing contrast enhancing brain tumors and regions of peritumoral edema. J Magn Reson Imaging 2005;21:701-8.
109. Server A, Kulle B, Maehlen J, et al. Quantitative apparent diffusion coefficients in the characterization of brain tumors and associated peritumoral edema. Acta Radiol 2009;50:682-9.
110. Smith JS, Cha S, Mayo MC, et al. Serial diffusion-weighted magnetic resonance imaging in cases of glioma: distinguishing tumor recurrence from postresection injury. J Neurosurg 2005;103:428-38.
111. Jain R, Scarpace LM, Ellika S, et al. Imaging response criteria for recurrent gliomas treated with bevacizumab: role of diffusion weighted imaging as an imaging biomarker. J Neurooncol 2010;96:423-31.
112. Pope WB, Qiao XJ, Kim HJ, et al. Apparent diffusion coefficient histogram analysis stratifies progression-free and overall survival in patients with recurrent GBM treated with bevacizumab: a multi-center study. J Neurooncol 2012;108:491-8.
113. Lee WJ, Choi SH, Park CK, et al. Diffusion-weighted MR imaging for the differentiation of true progression from pseudoprogression following concomitant radiotherapy with temozolomide in patients with newly diagnosed high-grade gliomas. Acad Radiol 2012;19:1353-61.
114. Matsusue E, Fink JR, Rockhill JK, Ogawa T, Maravilla KR. Distinction between glioma progression and post-radiation change by combined physiologic MR imaging. Neuroradiology 2010;52:297-306.
115. Okada T, Mikuni N, Miki Y, et al. Corticospinal tract localization: integration of diffusion-tensor tractography at 3-T MR imaging with intraoperative white matter stimulation mapping--preliminary results. Radiology 2006;240:849-57.
116. Haris M, Kumar S, Raj MK, et al. Serial diffusion tensor imaging to characterize radiation-induced changes in normal-appearing white matter following radiotherapy in patients with adult low-grade gliomas. Radiat Med 2008;26:140-50.
117. Kitahara S, Nakasu S, Murata K, Sho K, Ito R. Evaluation of treatment-induced cerebral white matter injury by using diffusion-tensor MR imaging: initial experience. AJNR Am J Neuroradiol 2005;26:2200-6.
118. Aronen HJ, Gazit IE, Louis DN, et al. Cerebral blood volume maps of gliomas: comparison with tumor grade and histologic findings. Radiology 1994;191:41-51.
119. Knopp EA, Cha S, Johnson G, et al. Glial neoplasms: dynamic contrast-enhanced T2*-weighted MR imaging. Radiology 1999;211:791-8.
120. Lev MH, Ozsunar Y, Henson JW, et al. Glial tumor grading and outcome prediction using dynamic spin-echo MR susceptibility mapping compared with conventional contrast-enhanced MR: confounding effect of elevated rCBV of oligodendrogliomas [corrected]. AJNR Am J Neuroradiol 2004;25:214-21.
121. Cha S, Tihan T, Crawford F, et al. Differentiation of low-grade oligodendrogliomas from low-grade astrocytomas by using quantitative blood-volume measurements derived from dynamic susceptibility contrast-enhanced MR imaging. AJNR Am J Neuroradiol 2005;26:266-73.
122. Law M, Yang S, Babb JS, et al. Comparison of cerebral blood volume and vascular permeability from dynamic susceptibility contrast-enhanced perfusion MR imaging with glioma grade. AJNR Am J Neuroradiol 2004;25:746-55.
123. Cha S, Knopp EA, Johnson G, Wetzel SG, Litt AW, Zagzag D. Intracranial mass lesions: dynamic contrast-enhanced susceptibility-weighted echo-planar perfusion MR imaging. Radiology 2002;223:11-29.
124. Barajas RF, Chang JS, Sneed PK, Segal MR, McDermott MW, Cha S. Distinguishing recurrent intra-axial metastatic tumor from radiation necrosis following gamma knife radiosurgery using dynamic susceptibility-weighted contrast-enhanced perfusion MR imaging. AJNR Am J Neuroradiol 2009;30:367-72.
125. Barajas RF Jr, Chang JS, Segal MR, et al. Differentiation of recurrent glioblastoma multiforme from radiation necrosis after external beam radiation therapy with dynamic susceptibility-weighted contrast-enhanced perfusion MR imaging. Radiology 2009;253:486-96.
126. Roberts HC, Roberts TP, Ley S, Dillon WP, Brasch RC. Quantitative estimation of microvascular permeability in human brain tumors: correlation of dynamic Gd-DTPA-enhanced MR imaging with histopathologic grading. Acad Radiol 2002;9 Suppl 1:S151-5.
127. Roberts HC, Roberts TP, Bollen AW, Ley S, Brasch RC, Dillon WP. Correlation of microvascular permeability derived from dynamic contrast-enhanced MR imaging with histologic grade and tumor labeling index: a study in human brain tumors. Acad Radiol 2001;8:384-91.
128. Roberts HC, Roberts TP, Brasch RC, Dillon WP. Quantitative measurement of microvascular permeability in human brain tumors achieved using dynamic contrast-enhanced MR imaging: correlation with histologic grade. AJNR Am J Neuroradiol 2000;21:891-9.
129. Patankar TF, Haroon HA, Mills SJ, et al. Is volume transfer coefficient (K(trans)) related to histologic grade in human gliomas? AJNR Am J Neuroradiol 2005;26:2455-65.
130. Narang J, Jain R, Arbab AS, et al. Differentiating treatment-induced necrosis from recurrent/progressive brain tumor using nonmodel-based semiquantitative indices derived from dynamic contrast-enhanced T1-weighted MR perfusion. Neuro Oncol 2011;13:1037-46.
131. Horská A, Barker PB. Imaging of brain tumors: MR spectroscopy and metabolic imaging. Neuroimaging Clin N Am 2010;20:293-310.
132. Castillo M, Smith JK, Kwock L. Correlation of myo-inositol levels and grading of cerebral astrocytomas. AJNR Am J Neuroradiol 2000;21: 1645-9.
133. Howe FA, Barton SJ, Cudlip SA, et al. Metabolic profiles of human brain tumors using quantitative in vivo 1H magnetic resonance spectroscopy. Magn Reson Med 2003;49:223-32.
134. Haris M, Cai K, Singh A, Hariharan H, Reddy R. In vivo mapping of brain myo-inositol. Neuroimage 2011;54:2079-85.
135. Tien RD, Lai PH, Smith JS, Lazeyras F. Single-voxel proton brain spectroscopy exam (PROBE/SV) in patients with primary brain tumors. AJR Am J Roentgenol 1996;167:201-9.
136. McKnight TR, von dem Bussche MH, Vigneron DB, et al. Histopathological validation of a three-dimensional magnetic resonance spectroscopy index as a predictor of tumor presence. J Neurosurg 2002;97:794-

802.
137. Fountas KN, Kapsalaki EZ, Vogel RL, Fezoulidis I, Robinson JS, Gotsis ED. Noninvasive histologic grading of solid astrocytomas using proton magnetic resonance spectroscopy. Stereotact Funct Neurosurg 2004;82:90-7.
138. Huang Y, Lisboa PJ, El-Deredy W. Tumour grading from magnetic resonance spectroscopy: a comparison of feature extraction with variable selection. Stat Med 2003;22:147-64.
139. Server A, Josefsen R, Kulle B, et al. Proton magnetic resonance spectroscopy in the distinction of high-grade cerebral gliomas from single metastatic brain tumors. Acta Radiol 2010;51:316-25.
140. Plotkin M, Eisenacher J, Bruhn H, et al. 123I-IMT SPECT and 1H MR-spectroscopy at 3.0 T in the differential diagnosis of recurrent or residual gliomas: a comparative study. J Neurooncol 2004;70:49-58.
141. Träber F, Block W, Flacke S, et al. [1H-MR Spectroscopy of brain tumors in the course of radiation therapy: Use of fast spectroscopic imaging and single-voxel spectroscopy for diagnosing recurrence]. Rofo 2002;174:33-42.
142. Ando K, Ishikura R, Nagami Y, et al. [Usefulness of Cho/Cr ratio in proton MR spectroscopy for differentiating residual/recurrent glioma from non-neoplastic lesions]. Nihon Igaku Hoshasen Gakkai Zasshi 2004;64:121-6.
143. Hygino da Cruz LC Jr, Rodriguez I, Domingues RC, Gasparetto EL, Sorensen AG. Pseudoprogression and pseudoresponse: imaging challenges in the assessment of posttreatment glioma. AJNR Am J Neuroradiol 2011;32:1978-85.
144. Henry RG, Vigneron DB, Fischbein NJ, et al. Comparison of relative cerebral blood volume and proton spectroscopy in patients with treated gliomas. AJNR Am J Neuroradiol 2000;21:357-66.
145. Park I, Chen AP, Zierhut ML, Ozturk-Isik E, Vigneron DB, Nelson SJ. Implementation of 3 T lactate-edited 3D 1H MR spectroscopic imaging with flyback echo-planar readout for gliomas patients. Ann Biomed Eng 2011;39:193-204.
146. Li X, Vigneron DB, Cha S, et al. Relationship of MR-derived lactate, mobile lipids, and relative blood volume for gliomas in vivo. AJNR Am J Neuroradiol 2005;26:760-9.
147. Crawford FW, Khayal IS, McGue C, et al. Relationship of pre-surgery metabolic and physiological MR imaging parameters to survival for patients with untreated GBM. J Neurooncol 2009;91:337-51.
148. Nelson SJ, Vigneron D, Kurhanewicz J, Chen A, Bok R, Hurd R. DNP-Hyperpolarized C Magnetic Resonance Metabolic Imaging for Cancer Applications. Appl Magn Reson 2008;34:533-44.
149. Park I, Larson PE, Zierhut ML, et al. Hyperpolarized 13C magnetic resonance metabolic imaging: application to brain tumors. Neuro Oncol 2010;12:133-44.
150. Park I, Bok R, Ozawa T, et al. Detection of early response to temozolomide treatment in brain tumors using hyperpolarized 13C MR metabolic imaging. J Magn Reson Imaging 2011;33:1284-90.
151. Chaumeil MM, Larson PE, Yoshihara HA, et al. Non-invasive in vivo assessment of IDH1 mutational status in glioma. Nat Commun 2013;4:2429.
152. Lee MH, Smyser CD, Shimony JS. Resting-state fMRI: a review of methods and clinical applications. AJNR Am J Neuroradiol 2013;34:1866-72.
153. Fox MD, Snyder AZ, Vincent JL, Corbetta M, Van Essen DC, Raichle ME. The human brain is intrinsically organized into dynamic, anticorrelated functional networks. Proc Natl Acad Sci U S A 2005;102:9673-8.
154. De Luca M, Beckmann CF, De Stefano N, Matthews PM, Smith SM. fMRI resting state networks define distinct modes of long-distance interactions in the human brain. Neuroimage 2006;29:1359-67.
155. Biswal B, Yetkin FZ, Haughton VM, Hyde JS. Functional connectivity in the motor cortex of resting human brain using echo-planar MRI. Magn Reson Med 1995;34:537-41.
156. Binder JR, Swanson SJ, Hammeke TA, et al. Determination of language dominance using functional MRI: a comparison with the Wada test. Neurology 1996;46:978-84.
157. Adcock JE, Wise RG, Oxbury JM, Oxbury SM, Matthews PM. Quantitative fMRI assessment of the differences in lateralization of language-related brain activation in patients with temporal lobe epilepsy. Neuroimage 2003;18:423-38.
158. Vlieger EJ, Majoie CB, Leenstra S, Den Heeten GJ. Functional magnetic resonance imaging for neurosurgical planning in neurooncology. Eur Radiol 2004;14:1143-53.
159. Håberg A, Kvistad KA, Unsgård G, Haraldseth O. Preoperative blood oxygen level-dependent functional magnetic resonance imaging in patients with primary brain tumors: clinical application and outcome. Neurosurgery 2004;54:902-14; discussion 914-5.
160. Shimony JS, Zhang D, Johnston JM, Fox MD, Roy A, Leuthardt EC. Resting-state spontaneous fluctuations in brain activity: a new paradigm for presurgical planning using fMRI. Acad Radiol 2009;16:578-83.
161. Zhang D, Johnston JM, Fox MD, et al. Preoperative sensorimotor mapping in brain tumor patients using spontaneous fluctuations in neuronal activity imaged with functional magnetic resonance imaging: initial experience. Neurosurgery 2009;65(6 Suppl):226-36.
162. Kokkonen SM, Nikkinen J, Remes J, et al. Preoperative localization of the sensorimotor area using independent component analysis of resting-state fMRI. Magn Reson Imaging 2009;27:733-40.
163. Mickevicius N, Sabsevitz D, Bovi J, LaViolette PS. Effects of whole-brain radiation therapy on resting state connectivity: a case study. Int J Radiat Oncol Biol Phys 2014;90:S325.
164. Sours C, Mistry N, Zhang H, et al. Feasibility study testing the incorporation of resting state fMRI data in radiation therapy planning to limit dose to cognitive function networks in patients with primary brain tumors. Int J Radiat Oncol Biol Phys 2013;87:S254-5.
165. Harris RJ, Bookheimer SY, Cloughesy TF, et al. Altered functional connectivity of the default mode network in diffuse gliomas measured with pseudo-resting state fMRI. J Neurooncol 2014;116:373-9.
166. Werner P, Barthel H, Drzezga A, Sabri O. Current status and future role of brain PET/MRI in clinical and research settings. Eur J Nucl Med Mol Imaging 2015;42:512-26.
167. Puttick S, Bell C, Dowson N, Rose S, Fay M. PET, MRI, and simultaneous PET/MRI in the development of diagnostic and therapeutic strategies for glioma. Drug Discov Today 2014 Nov 6 [Epub]. http://dx.doi.org/10.1016/j.drudis.2014.10.016.
168. Ricci PE, Karis JP, Heiserman JE, Fram EK, Bice AN, Drayer BP. Differentiating recurrent tumor from radiation necrosis: time for re-evaluation of positron emission tomography? AJNR Am J Neuroradiol 1998;19:407-13.
169. Weber W, Bartenstein P, Gross MW, et al. Fluorine-18-FDG PET and iodine-123-IMT SPECT in the evaluation of brain tumors. J Nucl Med 1997;38:802-8.
170. Singhal T, Narayanan TK, Jacobs MP, Bal C, Mantil JC. 11C-methionine PET for grading and prognostication in gliomas: a comparison study with 18F-FDG PET and contrast enhancement on MRI. J Nucl Med 2012;53:1709-15.
171. Floeth FW, Pauleit D, Wittsack HJ, et al. Multimodal metabolic imaging of cerebral gliomas: positron emission tomography with [18F]fluoroethyl-L-tyrosine and magnetic resonance spectroscopy. J Neurosurg 2005;102:318-27.
172. Pauleit D, Floeth F, Hamacher K, et al. O-(2-[18F]fluoroethyl)-L-tyrosine PET combined with MRI improves the diagnostic assessment of cerebral gliomas. Brain 2005;128(Pt 3):678-87.
173. Pöpperl G, Kreth FW, Mehrkens JH, et al. FET PET for the evaluation of untreated gliomas: correlation of FET uptake and uptake kinetics with tumour grading. Eur J Nucl Med Mol Imaging 2007;34:1933-42.
174. Terakawa Y, Tsuyuguchi N, Iwai Y, et al. Diagnostic accuracy of 11C-methionine PET for differentiation of recurrent brain tumors from radiation necrosis after radiotherapy. J Nucl Med 2008;49:694-9.
175. Shishido H, Kawai N, Miyake K, Yamamoto Y, Nishiyama Y, Tamiya T. Diagnostic Value of 11C-Methionine (MET) and 18F-Fluorothymidine (FLT) Positron Emission Tomography in Recurrent High-Grade Glio-

mas; Differentiation from Treatment-Induced Tissue Necrosis. Cancers (Basel) 2012;4:244-56.
176. Chen W, Silverman DH, Delaloye S, et al. 18F-FDOPA PET imaging of brain tumors: comparison study with 18F-FDG PET and evaluation of diagnostic accuracy. J Nucl Med 2006;47:904-11.
177. Ledezma CJ, Chen W, Sai V, et al. 18F-FDOPA PET/MRI fusion in patients with primary/recurrent gliomas: initial experience. Eur J Radiol 2009;71:242-8.
178. Lizarraga KJ, Allen-Auerbach M, Czernin J, et al. (18)F-FDOPA PET for differentiating recurrent or progressive brain metastatic tumors from late or delayed radiation injury after radiation treatment. J Nucl Med 2014; 55:30-6.
179. Bruehlmeier M, Roelcke U, Schubiger PA, Ametamey SM. Assessment of hypoxia and perfusion in human brain tumors using PET with 18F-fluoromisonidazole and 15O-H2O. J Nucl Med 2004;45:1851-9.
180. Cher LM, Murone C, Lawrentschuk N, et al. Correlation of hypoxic cell fraction and angiogenesis with glucose metabolic rate in gliomas using 18F-fluoromisonidazole, 18F-FDG PET, and immunohistochemical studies. J Nucl Med 2006;47:410-8.
181. Szeto MD, Chakraborty G, Hadley J, et al. Quantitative metrics of net proliferation and invasion link biological aggressiveness assessed by MRI with hypoxia assessed by FMISO-PET in newly diagnosed glioblastomas. Cancer Res 2009;69:4502-9.
182. Hirata K, Terasaka S, Shiga T, et al. ^{18}F-Fluoromisonidazole positron emission tomography may differentiate glioblastoma multiforme from less malignant gliomas. Eur J Nucl Med Mol Imaging 2012;39:760-70.
183. Spence AM, Muzi M, Swanson KR, et al. Regional hypoxia in glioblastoma multiforme quantified with [18F]fluoromisonidazole positron emission tomography before radiotherapy: correlation with time to progression and survival. Clin Cancer Res 2008;14:2623-30.